Sensorimotor control of breathing in the *mdx* mouse model of Duchenne muscular dystrophy

David P. Burns[1], Arijit Roy[2], Eric F. Lucking[1], Fiona B. McDonald[2], Sam Gray[3], Richard J. Wilson[2], Deirdre Edge[3] and Ken D. O'Halloran[1,*]

[1]Department of Physiology, University College Cork, Cork, Ireland.

[2]Hotchkiss Brain Institute, University of Calgary, Calgary, Alberta, Canada.

[3]Department of Physiology, Trinity Biosciences Institute, Trinity College Dublin, the University of Dublin, Dublin, Ireland.

***Corresponding author:**

Professor Ken D. O'Halloran, PhD | Department of Physiology, Western Gateway Building, Western Road

Cork, Ireland | Tel: +353-21-4205433 | k.ohalloran@ucc.ie

Short title: *Hypoventilation in young* mdx *mice*

Abbreviations: AUC, area under the curve; CSA, cross-sectional area; CSN, carotid sinus nerve; CT, contraction time; DMD, Duchenne muscular dystrophy; EMG, electromyogram; f_R, respiratory frequency; F_iO_2, fractional inspired oxygen concentration; Hb, haemoglobin; HCO_3^-, bicarbonate; L_o, optimum length; MFO, mean frequency oscillation; PCO_2, partial pressure of CO_2; PO_2, partial pressure of O_2; P_t, isometric twitch force; SpO_2, arterial O_2 percent saturation; TCO_2, total CO_2; V_E, minute ventilation; V_E/VCO_2, ventilatory equivalent for CO_2; V_E/VO_2, ventilatory equivalent for O_2; VCO_2, carbon dioxide production; VO_2, oxygen consumption; V_T, tidal volume; ½ RT, half-relaxation time.

Key points

- Respiratory failure is a leading cause of mortality in Duchenne muscular dystrophy (DMD), but little is known about the control of breathing in DMD and animal models.

This is an Accepted Article that has been peer-reviewed and approved for publication in the The Journal of Physiology, but has yet to undergo copy-editing and proof correction. Please cite this article as an 'Accepted Article'; doi: 10.1113/JP274792.

- We show that young (8 weeks of age) *mdx* mice hypoventilate during basal breathing due to reduced tidal volume. Basal CO_2 production is equivalent in wild-type and *mdx* mice.

- We show that carotid bodies from *mdx* mice have blunted responses to hyperoxia, revealing hypoactivity in normoxia. However, carotid body, ventilatory and metabolic responses to hypoxia are equivalent in wild-type and *mdx* mice.

- Our study revealed profound muscle weakness and muscle fibre remodelling in young *mdx* diaphragm suggesting severe mechanical disadvantage in *mdx* mice at an early age.

- Our study reveals a potentiated neural motor drive to breathe in *mdx* mice during maximal chemoactivation, suggesting compensatory neuroplasticity enhancing respiratory motor output to the diaphragm and likely other accessory muscles.

Abstract

Patients with Duchenne muscular dystrophy (DMD) hypoventilate with consequential arterial blood gas derangement relevant to disease progression. Whereas deficits in DMD diaphragm are recognized, there is a paucity of knowledge in respect of the neural control of breathing in dystrophinopathies. We sought to perform an analysis of respiratory control in a model of DMD, the *mdx* mouse. In eight week old male wild-type and *mdx* mice, ventilation and metabolism, carotid body afferent activity, and diaphragm muscle force-generating capacity, and muscle fibre size, distribution and centronucleation were determined. Diaphragm EMG activity and responsiveness to chemostimulation was determined. During normoxia, *mdx* mice hypoventilated, owing to a reduction in tidal volume. Basal CO_2 production was not different between wild-type and *mdx* mice. Carotid sinus nerve responses to hyperoxia were blunted in *mdx* suggesting hypoactivity. However, carotid body, ventilatory and metabolic responses to hypoxia were equivalent in wild-type and *mdx* mice. Diaphragm force was severely depressed in *mdx* mice, with evidence of fibre remodelling and damage. Diaphragm EMG responses to chemoactivation were enhanced in *mdx* mice. We conclude that there is evidence of chronic hypoventilation in young *mdx* mice. Diaphragm dysfunction confers mechanical deficiency in *mdx* resulting in impaired capacity to generate normal tidal volume at rest and decreased absolute ventilation during chemoactivation. Enhanced *mdx* diaphragm EMG responsiveness suggests compensatory neuroplasticity facilitating respiratory motor output, which may extend to accessory muscles of breathing. Our results may have relevance to emerging treatments for human DMD aiming to preserve ventilatory capacity.

Keywords: Duchenne muscular dystrophy, *mdx*, hypoventilation, carotid body, diaphragm, EMG

Abstract word count= 245

1. Introduction

Duchenne muscular dystrophy (DMD) is a fatal X-linked neuromuscular disease characterized by dystrophin deficiency. Deficits in this structural protein lead to aberrant structural remodelling and damage in skeletal and other muscles (Muntoni *et al.*, 2003; Deconinck & Dan, 2007; Ervasti, 2007; Mosqueira *et al.*, 2013b), with consequential profound muscle weakness extending to the striated muscles of breathing—the final effectors in the respiratory control network. Respiratory insufficiency is a hallmark of DMD (Baydur *et al.*, 1990; Bersanini *et al.*, 2012). Whereas diaphragm dysfunction is a recognized primary morbid feature in DMD (De Bruin *et al.*, 1997; Beck *et al.*, 2006; Khirani *et al.*, 2014), there is a paucity of knowledge in respect of the neural control of breathing in the human dystrophinopathies. Of note, DMD patients hypoventilate with resultant hypoxaemia (Smith *et al.*, 1989a, b; Melacini *et al.*, 1996), a symptom which may have particular relevance to muscle pathology and disease progression, in the light of data from rodent models revealing hypoxia-induced respiratory muscle weakness (McMorrow *et al.*, 2011; Skelly *et al.*, 2012; Shortt *et al.*, 2014) due to altered redox signalling and overt oxidative stress (Lewis *et al.*, 2015; Lewis *et al.*, 2016), which are features of DMD.

Respiratory failure in DMD results in premature death. Yet, the early impact of dystrophin deficiency on the respiratory control network is unclear. This knowledge gap is significant and has potential relevance to the treatment of DMD. It is not known if dystrophin deficiency has consequences for sensorimotor control of breathing. There is ample evidence in support of remarkable capacity for plasticity within the respiratory control network governing arterial blood gas and pH homeostasis in health and disease (Mitchell & Johnson, 2003; Kumar & Prabhakar, 2012; Fuller & Mitchell, 2017). Sensory and motor plasticity is context-dependent, with a capacity for adaptive or maladaptive outcomes. Compensatory neuroplasticity at one or more sites of the respiratory control network could ameliorate respiratory muscle deficits in early stages of DMD. Conversely, sensorimotor deficits could exacerbate aberrant respiratory control in DMD and contribute to disease progression. Dystrophin is present in the carotid body (Mosqueira *et al.*, 2013a), the primary blood oxygen sensor, but it is unclear if dystrophin deficiency affects chemoafferent discharge and as such, the control of breathing. Dystrophin is also present in neurons (Lidov, 1996), but it is not known if central respiratory motor drive is affected by dystrophinopathies, potentiating or ameliorating

impaired respiratory mechanics due to respiratory muscle weakness. A greater understanding of the control of breathing in DMD is likely to prove important to therapeutic strategies, and might offer novel targets in interventional therapies particularly early in disease onset before the establishment of overt respiratory pathology.

We sought to perform an assessment of respiratory control in a young murine model of DMD—the *mdx* mouse. Whereas, diaphragm dysfunction faithfully recapitulating the human condition has been established in the model, assessment of respiratory control, especially in young animals, is lacking. We hypothesized that there should be evidence of neuroplasticity in the respiratory control network of the *mdx* mouse.

2. Methods

2.1 Ethical approval

Procedures concerning live animals were performed under licence in accordance with Irish and European directive 2010/63/EU following approval by University College Cork animal research ethics committee. Carotid body recordings were performed in accordance with The Canadian Council on Animal Care Guidelines and were approved locally by the Animal Care Committee of the Cumming School of Medicine, University of Calgary, Canada.

2.2 Experimental Animals

Male and female wild-type (C57BL/10ScSnJ) and *mdx* (C57BL/10ScSn-Dmd^{mdx}/J) mice were purchased from the Jackson Laboratory (Bar Harbor, ME, USA) and bred at University College Cork's animal housing facility. Eight week old male wild-type (n=53) and *mdx* (n=52) mice were studied for respiratory and metabolism measurements, *ex vivo* muscle function tests, tissue harvesting for immunohistochemistry, *in vivo* EMG recordings and arterial blood gas analysis. For carotid body-carotid sinus nerve preparations, male wild-type (n=6) and *mdx* (n=6) mice were purchased from the Jackson Laboratory and transferred to the University of Calgary for subsequent experiments at eight weeks of age. Animals were housed conventionally in temperature- and humidity-controlled facilities, operating on a 12 h light: 12 h dark cycle with food and water available *ad libitum*.

2.3 Respiratory recordings

Respiratory flow recordings were performed using whole-body plethysmography in unrestrained, unanaesthetized mice during quiet rest. Wild-type (n=13) and *mdx* (n=12) mice were introduced into plethysmograph chambers (Model PLY4211; volume=0.6L, Buxco Research Systems, Wilmington, NC,

USA) and allowed a 60-90 minute acclimation period until sufficiently settled, with room air passing through each chamber (1 L/min). Recordings were typically performed in parallel, with contemporaneous assessment of breathing in one wild-type mouse and one *mdx* mouse using a two chamber set-up. For successive recording sessions, mice were assigned to chambers based on genotype in an alternating fashion to avoid any potential bias associated with a given chamber. Post hoc analysis of breathing within each genotype confirmed no difference in parameters recorded comparing data derived from the two chambers. *Experimental protocol:* Following the acclimation period, a 20-30 minute baseline recording was performed in normoxia. This was followed by a 20 minute hypoxic challenge (F_iO_2=0.1; balance N_2). Following a 60 minute recovery period in normoxia, a 20-30 minute normoxic baseline period was recorded. This was followed by a graded hypoxic challenge in which animals were challenged with decreasing levels of inspired oxygen: F_iO_2=0.15, 0.12, 0.10, and 0.08 (balance N_2) consecutively for 5 minutes each. Respiratory parameters including respiratory frequency (f_R), tidal volume (V_T) and minute ventilation (V_E) were recorded on a breath-by-breath basis for analysis offline. *Data analysis:* To maximize the recording period for the assessment of ventilatory parameters in normoxia, both normoxic bouts were pooled to generate one set of baseline (normoxia) data; there was no significant difference for ventilatory parameters between the two normoxic periods. Based on the time constant for the plethysmograph chambers and that gases were thoroughly mixed before entry to the plethysmograph chambers, we assumed complete gas mixing during gas challenges by ~3 minutes of exposure. For the sustained (20 minute) hypoxic challenge, data are shown after 5 minutes of exposure and are presented on a minute-by-minute basis thereafter. For the graded hypoxic challenge, measurements were taken during the 5th minute of exposure to the given F_iO_2 challenge. For each of the hypoxic challenges (sustained and graded), data during hypoxic exposure were compared with the preceding 5 minutes of baseline (F_iO_2: 0.21). In a separate historical cohort of wild-type (n=10) and *mdx* (n=11) mice (Burns *et al.*, 2015), we assessed the ventilatory response to a 10 minute hypercapnic gas challenge (5% CO_2, balance O_2). V_T and V_E were normalized for body mass (g).

2.4 Metabolism measurements

O_2 consumption (VO_2) and CO_2 production (VCO_2) were measured in wild-type (n=13) and *mdx* (n=12) mice undergoing the whole-body plethysmography protocol. Airflow through the chamber was maintained at 1 L/min. Fractional concentrations of O_2 and CO_2 were measured in air entering and exiting the plethysmograph (O_2 and CO_2 analyzer; ADInstruments, Colorado Springs, CO, USA) similar to that previously described (Bavis *et al.*, 2010; Bavis *et al.*, 2014). *Data analysis:* calculation of VO_2 and VCO_2 was performed as previously described (Haouzi *et al.*, 2009). For the sustained (20

minute) hypoxic challenge data are shown after 5 minutes of exposure and are presented on a minute-by-minute basis thereafter. For the graded hypoxic challenge, measurements were taken during the 5th minute of exposure to the given F_iO_2 challenge. For each of the hypoxic challenges (sustained and graded), data during hypoxic exposure were compared with the preceding 5 minutes of baseline (F_iO_2: 0.21). VO_2 and VCO_2 were normalized for body mass (g).

2.5 Blood gas analysis

Wild-type (n=7) and *mdx* (n=7) mice were anaesthetized with 5% isoflurane in air. A laparotomy was performed and cardiac puncture was performed by advancing a 25G needle through the diaphragm and into the apex of the heart for blood sampling for analysis. 0.2ml of blood was collected and used to measure pH, the partial pressure of O_2 (PO_2) and CO_2 (PCO_2), total CO_2 (TCO_2), bicarbonate concentration [HCO_3^-], arterial saturation (SaO_2), sodium ion concentration [Na^+], potassium ion concentration [K^+], haematocrit and haemoglobin concentration [Hb] using a blood gas analyzer (i-Stat; Heska, Fort Collins, CO, USA). Euthanasia was confirmed with cervical dislocation.

2.6 Arterially perfused ex vivo *carotid body-carotid sinus nerve preparation*

At the University of Calgary, wild-type (n=6) and *mdx* (n=6) mice were heavily anaesthetized with isoflurane and then decapitated (lower cervical level). The carotid bifurcation, including the carotid body-carotid sinus nerve-superior cervical ganglion, was quickly isolated *en bloc* for *in vitro* perfusion as described previously (Roy *et al.*, 2012). The carotid bifurcation was then transferred to a dissection dish containing physiological saline (in mM: 1 $MgSO_4$, 1.25 NaH_2PO_4, 4 KCl, 24 $NaHCO_3$, 115 NaCl, 10 glucose, 12 sucrose, and 2 $CaCl_2$) and equilibrated with hyperoxia (95% O_2/5% CO_2). After 15-20 min, the isolated tissue was transferred to a recording chamber with a built-in water-fed heating circuit and the common carotid artery was immediately cannulated for luminal perfusion with physiological saline equilibrated with 100 mmHg PO_2 and 36 mmHg PCO_2 (balance N_2). The carotid sinus nerve was then carefully desheathed and the carotid sinus region was bisected. The occipital, internal, and external arteries were ligated, and small incisions were made on the internal and external carotid arteries to allow perfusate to exit. A peristaltic pump was used to set the perfusion rate at ~10 ml/min, which was sufficient to maintain a constant pressure of 90-100 mmHg at the tip of the cannula. The perfusate was equilibrated with computer-controlled gas mixtures monitored using CO_2 and O_2 gas analyzers (models CA-2A and PA1B, respectively, Sable Systems, Las Vegas, NV, USA); a gas mixture of 100 mmHg PO_2 and 36 mmHg PCO_2 (balance N_2) was used to start the experiments (yielding pH ~7.4). Before reaching the cannula, the perfusate was passed through a bubble trap and heat exchanger. The temperature of the perfusate, measured continuously as it

departed the preparation, was maintained at 37±0.5°C. The effluent from the chamber was recirculated.

Chemosensory discharge was recorded extracellularly from the whole desheathed carotid sinus nerve, which was placed on a platinum electrode and lifted into a thin film of paraffin oil. A reference electrode was placed close to the bifurcation. Carotid sinus nerve activity was monitored using a differential AC amplifier (model 1700, AM Systems) and a secondary amplifier (model AM502, Tektronix, Beaverton, OR). The neural activity was amplified, filtered (300-Hz low cutoff, 5-kHz high cutoff), displayed on an oscilloscope, rectified, integrated (200-ms time constant), and stored on a computer using an analogue-to-digital board (Digidata 1322A, Axon Instruments) and data acquisition software (Axoscope 9.0). Preparations were left undisturbed for 45 min to stabilize before the experimental protocol began. *Experimental protocol:* The following protocol was used for all experiments: 1) the carotid body was perfused for 5 min with normoxia (100 mmHg PO_2 and 36 mmHg PCO_2; balance N_2) to determine baseline carotid sinus nerve activity; 2) neural responses were obtained by challenging the carotid body for 5 min with mild, moderate and severe hypoxia (80, 60 & 40 mmHg, respectively) interspersed with normoxia; 3) finally a hyperoxic (500 mmHg PO_2 and 36 mmHg PCO_2; balance N_2) challenge was given for 5 min to examine the sensitivity of the carotid body (Dejours test). *Data analysis:* Data were analyzed offline using custom software (written by R.J.A. Wilson). Carotid sinus nerve activity was divided into 2s time bins, and activity in each bin was rectified and summed (expressed as integrated neural discharge). Data are shown as absolute carotid sinus nerve discharge frequencies in each of the different conditions in the protocol. Neural responses to PO_2 challenge were determined by comparing absolute discharge frequencies and also responses normalized to the hyperoxic condition, and separately to the normoxic condition.

2.7 Ex vivo *muscle function tests*

Diaphragm muscle function was examined *ex vivo* under isometric conditions using a standardized protocol as previously described (Shortt *et al.*, 2014). Wild-type (n=7) and *mdx* (n=7) mice were anaesthetized with 5% isoflurane by inhalation in air and euthanized by cervical dislocation. The diaphragm muscle was excised immediately with rib and central tendon attached. Longitudinally arranged bundles were prepared for assessment of contractile function and were suspended vertically between two platinum plate electrodes. The rib was attached to a fixed hook at one end and the central tendon was attached to a force transducer with non-elastic string at the other end. Muscle baths contained Krebs solution (in mM: 120 NaCl, 5 KCl, 2.5 Ca^{2+}, 1.2 $MgSO_4$, 1.2 NaH_2PO_4, 25 $NaHCO_3$, 11.5 glucose) and D-tubocurarine (25µM) and were equilibrated under hyperoxic conditions

(95% O_2/ 5% CO_2). The optimum length (L_o) was determined by adjusting the position of the force transducer, and hence the length of the muscle preparations, by use of a micro-positioner between intermittent twitch contractions (Burns & O'Halloran, 2016; Burns *et al.*, 2017). L_o was taken as the muscle length associated with maximal isometric twitch force in response to single isometric twitch stimulation (supramaximal stimulation, 1ms duration). Once L_o was determined, the muscle was held at this length for the duration of the protocol. *Experimental protocol:* A single isometric twitch was measured. Peak isometric twitch force (P_t), contraction time (CT; time to peak force) and half-relaxation time (½ RT; time for peak force to decay by 50%) were determined. The force-frequency relationship was determined by sequentially stimulating the muscle at 10, 20, 40, 60, 80, 100, 120, 140, 160 Hz (300ms train duration), allowing a 1 min interval between stimulation. *Data analysis:* Specific force was calculated in N/cm^2 of muscle cross-sectional area (CSA). The CSA of each strip was determined by dividing the muscle mass (weight in grams) by the product of muscle L_o (cm) and muscle density (assumed to be 1.06 g/cm^3). The CT and ½ RT were measured as indices of isometric twitch kinetics. Normalization of diaphragm forces to CSA was principally a means of standardizing the *ex vivo* muscle preparations. It should be noted that tissue, and not muscle fibre CSA was estimated with this approach and our data do not provide information on the specific force of muscle fibres *per se*, which might also require consideration of revised muscle density values in *mdx*. Absolute muscle forces (N) were also assessed and compared in our study.

2.8 Muscle immunohistochemistry

Wild-type (n=8) and *mdx* (n=8) mice were anaesthetized with 5% isoflurane by inhalation in air and euthanized by cervical dislocation. Diaphragm muscle was excised immediately and a section of the hemi-diaphragm was mounted on a block of liver. Tissue samples were embedded in optimum cutting temperature (OCT; VWR International, Dublin, Ireland) embedding medium, frozen in isopentane (Sigma Aldrich, Wicklow, Ireland) cooled in liquid nitrogen and stored at -80^{o}C for subsequent structural analysis. Serial transverse muscle sections (10µm) were cryosectioned (Leica CM3050; Leica Microsystems, Nussloch, Germany) at -22^{o}C and mounted on polylysine-coated glass slides (VWR International, Dublin, Ireland). Slides were immersed in PBS (0.01 M) containing 1% bovine serum albumin (BSA) for 15 minutes. After 3x5 minute PBS washes, slides were immersed in PBS containing 5% normal goat serum (Sigma Aldrich, Wicklow, Ireland) for 30 minutes. Slides then underwent a further 3x5 minute PBS washes prior to application of the primary antibody (rabbit anti-laminin, 1:500; Sigma Aldrich, Wicklow, Ireland), diluted in PBS and 1% BSA. Slides were incubated overnight at 4^{o}C in a humidity chamber. After the incubation period, slides were washed with PBS for 3x5 minutes before the secondary antibody (FITC-conjugated goat anti-rabbit; 1.250,

Sigma Aldrich, Wicklow, Ireland), diluted in PBS and 1% BSA, was applied. Slides were incubated for 1 hour in the dark at room temperature. To identify myonuclei, the nuclear stain Hoechst (Sigma Aldrich, Wicklow, Ireland) was diluted in PBS (1:4) and applied to a subset of muscle sections for 10 minutes. Slides were rinsed with PBS for 5 minutes, cover-slipped with polyvinyl alcohol mounting medium with DABCO® anti-fade (Sigma Aldrich, Wicklow, Ireland). *Data analysis*: Muscle sections were viewed at x10 magnification and images captured using an Olympus BX51 microscope and an Olympus DP71 camera. For each animal, 3-4 images were captured for analysis from multiple muscle sections. For measurements, a square test frame of (600 x 600 µm), with inclusion and exclusion boundaries, was placed randomly over each image (Shortt et al., 2014). To determine the size distribution of muscle fibres within the diaphragm the individual fibre boundaries were determined using Imaris software. From this, the fibre cross-sectional area as well as Feret's minimal diameter were determined (Dubach-Powell, 2008). The coefficient of variation of muscle fibre minimal Feret's diameter, was also constructed for wild-type and *mdx*. In a subset of animals (n=5 per genotype) centrally nucleated muscle fibres were identified using ImageJ software on merged laminin and hoescht stained images. The proportion of centrally nucleated muscle fibres was expressed relative to the total number of myofibres analyzed per image. Data generated from multiple images was averaged per animal before computing group means.

2.9 Diaphragm EMG activity and responsiveness

Anaesthesia was induced with 5% isoflurane in 60% O_2 (balance N_2) followed by urethane (1.8 g/kg i.p.). Wild-type (n=8) and *mdx* (n=7) mice were then placed in the supine position, gradually weaned off the isoflurane and body temperature was maintained at 37^{o}C via a rectal probe and thermostatically-controlled heating blanket (Harvard Apparatus, Holliston, MA, USA). Supplemental anaesthetic was administered if necessary to maintain a surgical plane of anaesthesia, which was assessed by assessment of pedal withdrawal reflex to noxious pinch. A pulse oximeter clip (MouseOx™, Starr Life Sciences Corporation, Oakmount, PA, USA) was placed on the thigh of each mouse for the measurement of arterial O_2 saturation. A mid-cervical tracheotomy was performed to avoid upper airway obstruction. All animals were maintained with a bias flow of supplemental O_2 (FiO_2 = 0.60) unless otherwise stated. Concentric needle electrodes (26G; Natus Manufacturing Ltd, Ireland) were inserted into the costal diaphragm for the continuous measurement of diaphragm EMG activity which was amplified (x5,000), filtered (500Hz low cut-off to 5,000Hz high cut-off) and integrated (50ms time constant; Neurolog system, Digitimer Ltd, UK). All signals were passed through an analogue-to-digital converter (r8/30; ADInstruments, Colorado Springs, CO, USA) and were acquired using LabChart 7 (ADInstruments, Colorado Springs, CO, USA). *Experimental protocol:*

Spontaneously breathing animals were vagotomized and allowed to stabilize for a minimum of 5 minutes before baseline parameters were measured. It is established that chemostimulation in spontaneously breathing mice elicits a significantly greater phrenic motor response following vagotomy compared with vagi intact (Kline *et al.*, 2002). Next, animals were sequentially challenged with hypercapnia (5% CO_2 and 10% CO_2; 2min each), hypoxia (15% O_2; 1min), and asphyxia (15% O_2/5% CO_2; 1min) to examine the effects of chemostimulation on diaphragm EMG activity. Following completion of diaphragm EMG recordings, animals were euthanized via cervical dislocation. *Data analysis*: Amplitude and area under the curve (AUC) of integrated respiratory EMG activity was analyzed and averaged under steady-state basal conditions, and for 1 minute of baseline immediately prior to chemostimulation challenges. Amplitude and AUC of integrated respiratory EMG activity was analyzed and averaged for the final 15 breaths (maximal response) of the chemostimulation challenges. Baseline data were reported in absolute units. Responses to chemostimulation were expressed as percent change from the preceding baseline value. This portrayal of the data was considered appropriate given that baseline EMG activity was found to be equivalent in wild-type and *mdx* mice. As such, percent change from baseline is in effect equivalent to ΔEMG activity and importantly, a difference in the percent change between groups corresponds to a true difference in total EMG activity, important in the context of a transduction of neuromuscular-to-mechanical activity. Because we tested the hypothesis that diaphragm EMG activity would be altered in *mdx* mice compared with wild-type mice we did not normalize EMG data to a maximum reference value within each preparation (e.g. augmented breath or swallow), because such a maximum value could itself be changed in *mdx* mice resulting from neuroplasticity. Our principal focus was the level of EMG activity *per se*. In 1 *mdx* and 2 wild-type mice, the EMG response to gas challenges was characterized by tachypnoea and reduced EMG amplitude. Since our aim was to compare the magnitude of the increase in EMG amplitude (motor recruitment) during chemostimulation, we established *a priori* that trials characterized by frequency-only responses to gas challenge (tachypnoea) would be excluded from group analysis of the effects of chemostimulation on EMG amplitude and area under the curve in wild-type and *mdx* mice.

2.10 Statistical Analysis

Values are expressed as mean±SD or as box and whiskers plot (median, 25-75% centiles and minimum and maximum values). Data were statistically analyzed by Prism 6.0 (Graphpad Software, San Diego, CA, USA). For measures of baseline ventilation and metabolism, basal carotid sinus nerve activity during normoxia and hyperoxia, basal diaphragm EMG activity, diaphragm muscle twitch force and contractile kinetics, diaphragm muscle fibres, and arterial blood gas analysis, all data for wild-type and *mdx* groups were tested for normal distribution and equal variances and were

statistically compared using unpaired two-tailed Student *t* tests, with Welch's correction for unequal variances used as appropriate. Ventilatory and metabolic responsiveness to hypoxia (separate sustained and graded challenges), carotid sinus nerve activity response to hypoxic challenge, diaphragm muscle force-frequency relationship, and diaphragm EMG responses to chemostimulation in wild-type and *mdx* groups were statistically compared by repeated measures two-way ANOVA (gas x gene) with Bonferroni post hoc test. Data for absolute carotid sinus nerve activity were non-parametric and therefore were log transformed. $P < 0.05$ was considered statistically significant in all tests.

3. Results

3.1 Baseline ventilation and metabolism

Representative respiratory flow traces for wild-type and *mdx* mice during baseline (normoxic) ventilation are shown in Fig. 1A. Minute ventilation during baseline conditions (combined normoxic bouts) was significantly reduced in *mdx* compared with wild-type mice ($P = 0.0001$; unpaired Student *t* test; Fig. 1D). This reduction in normoxic V_E in *mdx* mice was the result of a lower V_T ($P = 0.0003$; Fig. 1C); f_R did not differ significantly between groups ($P = 0.2612$; Fig. 1B). Performing this analysis on absolute volume data (not normalized for body mass) yielded similar effects for both V_E and V_T (data not shown). Respiratory and metabolic parameters are shown in Table 1. Assessment of O_2 consumption (VO_2) and CO_2 production (VCO_2) revealed minimal differences between wild-type and *mdx* mice. VO_2 (normalized to body mass) was significantly reduced for *mdx* ($P = 0.0043$) compared with wild-type, but not when expressed in absolute terms of oxygen consumed ($P = 0.6985$). No difference was noted for VCO_2 between groups when analysis was performed on absolute and normalized values. Carbon dioxide production, chosen *a priori* as the preferred index of metabolism, was effectively unchanged between wild-type and *mdx* mice. The ventilatory equivalent for CO_2 (V_E/VCO_2) was significantly reduced for *mdx* ($P = 0.0243$) compared with wild-type mice, indicative of hypoventilation in *mdx* mice. The ratio of VCO_2 to VO_2 (respiratory exchange ratio) was not different between groups.

3.2 Blood gas analysis

Intra-cardiac blood gas data for wild-type and *mdx* mice are shown in Table 2. Haematocrit was significantly lower in *mdx* ($P = 0.0005$; unpaired Student *t* test) compared with wild-type, but haemoglobin concentration was equivalent between the two groups. Significant increases in blood values for $[HCO_3^-]$ ($P = 0.0496$), TCO_2 ($P = 0.00382$), $[K^+]$ ($P = 0.0078$), and $[Na^+]$ ($P = 0.0442$) were observed in *mdx* compared with wild-type.

3.3 Carotid sinus nerve discharge

Figure 2 shows representative traces from wild-type (A) and *mdx* (B) carotid body-carotid sinus nerve preparations *ex vivo*. Group data for carotid sinus nerve activity (normalized to hyperoxia) for wild-type and *mdx* preparations during normoxia (100 mmHg) and in response to a graded hypoxic challenge (80, 60 and 40 mmHg) are shown in Fig. 2C. Of note during normoxia, carotid sinus nerve activity was ~30% less in *mdx* compared with wild-type preparations (P = 0.0064; unpaired Student *t* test), revealing a relative hypoactivity of carotid body afferent discharge in normoxia. Both wild-type and *mdx* preparations responded to decreasing levels of O_2 by corresponding increases in carotid sinus nerve activity (P < 0.0001; two-way ANOVA); however, no significant difference in hypoxic responsiveness was noted between wild-type and *mdx* (gas x gene P = 0.6452). Statistical judgment of the data was equivalent whether normalized to hyperoxia or normoxia. Data for absolute carotid sinus nerve discharge frequencies in each condition are shown in Table 3. Consistent with the normalized data, there was no statistical difference in hypoxic responsiveness between wild-type and *mdx* preparations (Table 3). The carotid sinus nerve discharge frequency response to hyperoxia (Dejours test) was significantly blunted in *mdx* compared with wild-type (-18.7±7.2 vs. -7.7±3.1 ∆impulses per min, unpaired Student *t* test, P = 0.011 for wild-type (n=6) vs. *mdx* (n=6) mice), further suggestive of a relative hypoactivity during normoxia in *mdx* carotid body.

3.4 Ventilatory responsiveness to hypoxia and hypercapnia

Figure 3 shows ventilatory and metabolic data during normoxia and in response to graded hypoxia. Minute ventilation was lower in *mdx* (P = 0.0054; two-way ANOVA) compared with wild-type, attributed to a lower tidal volume in *mdx* mice. VCO_2 decreased in response to hypoxia in wild-type and *mdx* mice (P < 0.0001). V_E/VCO_2 increased for both wild-type and *mdx* mice with decreasing levels of inspired O_2 (P < 0.0001). No significant difference in V_E/VCO_2 was observed between wild-type and *mdx* mice in response to graded hypoxia. Fig. 4 shows the time course of minute ventilation to a 20 minute sustained hypoxic challenge (F_iO_2 = 0.1; balance N_2). Ventilation increased rapidly in wild-type and *mdx* mice at the onset of hypoxia (P < 0.0001) and then declined towards baseline values (Fig. 4). A significantly lower V_E in *mdx* compared with wild-type mice was observed during gas challenge (P = 0.03), owing to reduced V_T in *mdx* mice (Fig. 4). The peak hypoxic ventilatory response was not different between strains (delta V_E was +1.44±0.80 vs. +0.90±0.70 ml/min/g, unpaired Student *t* test, P = 0.07 for wild-type (n=13) vs. *mdx* (n=12); % change from baseline was +131.8±52.1% vs. +111.7±69.6%, P = 0.4185). Figure 5 shows data for V_E during baseline and hypercapnic gas challenge. Minute ventilation was increased significantly both in wild-type and *mdx* mice during CO_2 exposure. Minute ventilation remained significantly lower in *mdx* compared with

wild-type mice during hypercapnic breathing, but the ventilatory response to hypercapnia was not different between wild-type and *mdx* mice (delta V_E was +1.9±0.8 vs. +1.7±0.6 ml/min/g, unpaired Student *t* test, *P* = 0.5768 for wild-type (n=10) vs. *mdx* mice (n=11); % change from baseline was +131±47% vs. +178±80%, *P* = 0.1194).

3.5 Diaphragm muscle function

Representative original traces for wild-type and *mdx* diaphragm twitch contraction (A) and force-frequency relationship (B) are shown in Fig. 6. Isometric twitch force and contractile kinetics for wild-type and *mdx* mice are shown in Table 4. Twitch contraction time was significantly prolonged in *mdx* compared with wild-type diaphragms (*P* = 0.0155; unpaired Student *t* test). Twitch force was significantly reduced in *mdx* diaphragm muscle preparations (*P* = 0.0292). For force-frequency relationship, diaphragm specific force was significantly depressed in *mdx* compared with wild-type preparations (*P* = 0.0002, repeated measures two-way ANOVA). Post-hoc analysis revealed significant differences between wild-type and *mdx* diaphragm force generation across a broad stimulus range (40-160 Hz). Absolute measurements of diaphragm force (N), prior to normalization to CSA, were significantly depressed in *mdx* compared with wild-type.

3.6 Diaphragm muscle fibre size and distribution

Representative immunofluorescence images from wild-type and *mdx* diaphragm muscle are shown in figure 7. Dystrophin deficiency in *mdx* diaphragm resulted in a significant increase in the coefficient of variation of muscle fibre size (*P* < 0.0001; unpaired Student *t* test), as measured by minimal Feret's diameter (Fig. 7C). There was a significantly increased proportion of centralized myonuclei, indicative of muscle damage in *mdx* compared with wild-type (*P* = 0.0005; Fig. 7D). A leftward shift in the frequency distribution of muscle fibre size was evident in *mdx* diaphragm, based on minimal Feret's diameter (Fig. 7E) or CSA (Fig. 7F).

3.7 Diaphragm EMG responsiveness

Representative original diaphragm EMG traces during baseline and in response to chemostimulation are shown in figure 8A. Diaphragm EMG activity was examined in wild-type and *mdx* mice during baseline (60% O_2) and in response to chemostimulation challenges. Basal diaphragm EMG amplitude and AUC was not different between wild-type and *mdx* mice (Fig. 8B, inset). Gas challenges typically increased EMG responsiveness for both wild-type and *mdx* for amplitude (*P* = 0.0202; repeated measures two-way ANOVA; Fig. 8B) and AUC (*P* = 0.0531; Fig. 8C). For AUC, a significant genotype difference was noted (*P* = 0.0452) and post-hoc analysis revealed EMG responsiveness to maximal

chemostimulation (asphyxia) was significantly enhanced in *mdx* compared with wild-type mice ($P < 0.05$; two-way ANOVA with Bonferroni post-hoc test).

4. Discussion

The main findings of our study are: 1) young (eight week old) *mdx* mice hypoventilate during basal breathing, owing to reduced tidal volume; 2) intra-cardiac blood total CO_2 and [HCO_3^-] are elevated in young *mdx* mice suggesting compensated respiratory acidosis; 3) the carotid body response to hyperoxia is depressed in young *mdx* mice; 4) chemosensory, ventilatory, and metabolic responses to hypoxia are unaffected in young *mdx* mice; 5) there is profound diaphragm muscle weakness, fibre remodelling and damage in young *mdx* mice; 6) diaphragm EMG responsiveness to chemostimulation is enhanced in young *mdx* mice suggesting compensatory neuroplasticity.

Overall, our study revealed that basal CO_2 production was unaffected in *mdx* mice, but *mdx* mice had a substantial reduction in tidal volume that was not compensated for by increased breathing frequency resulting in reduced minute ventilation. Thus, *mdx* mice hypoventilate by 8 weeks of age i.e. inadequate ventilation to meet metabolic demand, which is suggested by the data for reduced ventilatory equivalent for carbon dioxide (V_E/VCO_2) in *mdx* mice. Cardiac puncture for blood gas analysis under isoflurane anesthesia (breathing air) revealed a trend towards decreased PO_2 and increased PCO_2 in *mdx*, but the changes were modest in comparison to the ventilatory data derived by plethysmography. There are at least three factors to consider. First, the blood was sampled from anaesthetized animals, and anaesthesia has pronounced inhibitory effects on ventilation, though this might be expected to potentiate respiratory depression in *mdx* mice. Second, there may be cardio-pulmonary adjustments that compensate for mechanical deficits in young *mdx* mice. Third, the sample size may have been too small to reveal statistical significance in some key parameters (PO_2 and PCO_2) that did change in a manner consistent with hypoventilation. Nonetheless, total CO_2 and [HCO_3^-] were significantly elevated in *mdx* mice suggesting the development of a compensated respiratory acidosis secondary to chronic hypoventilation. Persistent hypoventilation and resultant hypoxaemia, which have been described in *mdx* mice at 6 months of age (Mosqueira et al., 2013a), would be expected to cause increased haematocrit and haemoglobin concentration. Of interest, we noted significantly enlarged, darkened spleens in *mdx* mice, which may have implications for the control of circulating red blood cells. It would be interesting to determine if *mdx* mice are chronically hypoxic in early life, as hypoxic stress has the capacity to drive plasticity at multiple sites within the respiratory control network.

Sensory inputs from the peripheral chemoreceptors are generally regarded as providing a tonic drive to "eupnoeic" breathing. Moreover, while they primarily detect hypoxia, their sensitivity is strongly modulated by $PaCO_2$ and they have powerful non-linear interactions with central (brainstem) chemoreceptors that also detect CO_2 concentration (Wilson & Teppema, 2016). Therefore, the relative hypoactivity of *mdx* compared with wild-type carotid bodies might have contributed to the resting hypoventilation of *mdx* mice. Carotid body responses to hypoxia (mild, moderate and severe), whether assessed as absolute or normalized data, were equivalent in *mdx* and wild-type mice with no statistical genotype or genotype x gas effect. Of note, carotid sinus nerve afferent discharge was less at all PO_2 levels in *mdx* preparations, such that chemoafferent drive to the respiratory centres was lower in *mdx* compared with wild-type representing a potentially physiologically relevant sensory deficit in the control of breathing. Interestingly, ventilatory responsiveness to sustained and graded hypoxia was equivalent in *mdx* and wild-type mice with no genotype effect. Of note, however, ventilation was reduced in *mdx* due to significant reductions in tidal volume at all levels of hypoxic ventilation, which may relate to sensory deficit as well as mechanical disadvantage in *mdx* over a range of ventilations compared with wild-type. Metabolism and metabolic responses to hypoxia were generally equivalent between wild-type and *mdx* mice.

While our report is the first to characterize respiratory and metabolic parameters in young *mdx* mice and describe that a significant respiratory phenotype presents as early as 8 weeks of age, our data are generally consistent with reports of hypoventilation in older (6-12 months of age) *mdx* mice (Huang *et al.*, 2011; Mosqueira *et al.*, 2013a). When viewed together, the implication of these findings is that respiratory insufficiency presents early in the *mdx* model, and thus likely impacts on the progression and manifestation of respiratory morbidity typically reported in older animals.

Our study confirmed profound diaphragm weakness in *mdx* mice. Coirault et al. (1999) have previously reported reduced strength in *mdx* diaphragm which was associated with a reduction in the number of cross bridges generating contractile force and in the elementary force generated per actomyosin interaction. These functional changes were associated with changes in myosin isoform composition (shift from myosin heavy chain type IIX to IIA). Interestingly, diaphragm mechanical dysfunction is present at a young age (6 weeks) when muscle fibre necrosis and/or fibrosis remain limited (Coirault *et al.*, 2003). Diaphragm force-generating capacity in the present study was depressed across a broad range of stimulation frequencies including the range relevant to basal breathing. Respiratory nerve activity in mice displays medium frequency oscillations (MFOs) in the range of 20-50Hz (O'Neal *et al.*, 2005; ElMallah *et al.*, 2016), which are believed to reflect the underlying motor neuron discharge rates (Christakos *et al.*, 1991). The severe weakness in *mdx*

diaphragm at this early age appears primarily responsible for the mechanical disadvantage manifest in reduced tidal volumes in freely-behaving mice. Force increases as a function of stimulation frequency in *mdx* mice, which provides capacity to increase breathing in response to increased neural drive. However, the intrinsic weakness in *mdx* diaphragm is impressive even at this early stage, presumably placing a limit on ventilatory capacity. Moreover, force-generating capacity remains severely compromised at higher stimulation frequencies.

There are few studies examining the hypoxic ventilatory response in *mdx* (Mosqueira *et al.*, 2013a; Burns *et al.*, 2015). The hypometabolic response to hypoxia in mice is such that ventilatory responses to hypoxia are modest. Indeed, tidal volume and ventilation do not increase much above baseline in response to graded hypoxia, and the ventilatory response to sustained hypoxia is primarily driven by increased respiratory frequency. Therefore, it is difficult to discern from ventilatory responses to hypoxia if *mdx* mice are capable of transducing increased diaphragm force-generating capacity resulting from motor recruitment to increase ventilation. To examine this further, we assessed hypercapnic ventilatory responses in wild-type and *mdx* mice. Ventilation increased in response to hypercapnic challenge, due to increases in respiratory frequency and tidal volume, and the response was equivalent in the two groups. The data reveal that *mdx* mice are capable of increasing tidal volume during chemostimulation. Although, ventilation remains significantly lower in *mdx* compared with wild-type mice during hypercapnic breathing, the ventilatory response to hypercapnia is not different between the two groups of mice. This reveals an interesting feature of respiratory control in the young *mdx* mouse, namely that a considerable reserve in ventilatory capacity prevails, which presumably extends to accessory muscles of breathing given the profound weakness noted in the diaphragm muscle. Analysis of fibre size and distribution in diaphragm muscle revealed considerable fibre remodelling and evidence of centronucleation, which is a hallmark of fibre necrosis. Diaphragm muscle structure of *mdx* mice has been well described with muscle fibres undergoing inflammatory cell infiltration, fibrosis and necrosis (Gayraud *et al.*, 2007; Ishizaki *et al.*, 2008; Huang *et al.*, 2011). In addition to structural abnormalities in *mdx* resulting in loss of function, there is growing evidence implicating oxidative stress in dystrophic diaphragm pathology (Kim & Lawler, 2012; Kim *et al.*, 2013).

In anaesthetized mice, we examined respiratory neural drive to the diaphragm under baseline conditions and in response to chemostimulation with hypoxia, hypercapnia, and asphyxia. Baseline diaphragm EMG activity was equivalent in wild-type and *mdx* mice (although respiratory frequency was higher in *mdx* mice), but since anaesthetized animals breathed 60% oxygen under baseline conditions, it is likely that carotid body chemoafferent input was depressed in our studies such that

putative differences in peripheral control of breathing between *mdx* and wild-type (i.e. sensory deficit suggested by carotid body preparations) would not have contributed to the EMG findings. We further acknowledge the recognized limitations in respect of comparisons of EMG activity between animals. Whether dystrophin deficiency affects central respiratory motor outflow in normoxia was not established in our studies; however, given the significance of this observation, it is worthy of future investigation. Chemoactivation of diaphragm EMG activity was enhanced in *mdx,* with EMG activity considerably potentiated under maximal chemostimulation with asphyxia. The potentiated response, which revealed a true increase in absolute EMG activity, reveals compensatory plasticity in *mdx* either in the central brainstem respiratory network and/or at the level of the phrenic motor nucleus. Potentiated motor outflow in response to chemostimulation may serve to facilitate increased ventilation by providing greater neural drive via phrenic motor neurons to diaphragm, facilitating the transduction of neuromuscular-to-mechanical events during chemostimulation challenge. Perhaps in this manner the potentiated output facilitates equivalent increases in ventilation (delta V_E) during chemostimulation despite the mechanical disadvantage presenting in *mdx* mice.

However, it is important to recognize that the force-generating capacity of the *mdx* diaphragm is severely compromised. It is evident from analysis of force-frequency relationship in *mdx* diaphragm that increased frequency of stimulation results in little gain in force. As such, there may be little mechanical advantage to increased activation of the diaphragm, which suggests that activation of accessory muscles of breathing may be especially important in *mdx* (and DMD) to support increased tidal volume during respiratory stimulation. We acknowledge that aberrant motor unit potentials in dystrophic *mdx* muscle (Han *et al.*, 2006) could have contaminated diaphragm EMG recordings such that comparisons between wild-type and *mdx* may not be entirely appropriate in respect of the issue of neuroplasticity, an issue further complicated by potential changes at the neuromuscular junction (Pratt *et al.*, 2015). Recordings of phrenic motor discharge are required to definitively determine if central respiratory drive is elevated in *mdx* and this is an area worthy of future study. Assessment of motor drive in accessory pathways contributing to ventilation is also worthy of pursuit. It would also be very interesting to characterize motor unit potentials in respiratory EMGs of young *mdx* mice.

Limitations

Whole-body plethysmography provides an estimate of tidal volume, which is dependent on a number of assumptions (Mortola & Frappell, 1998; Stephenson & Gucciardi, 2002)). The calculation depends on knowledge of chamber temperature and humidity, and animal airway temperatures. Whereas the former were measured in our studies (~22^{o}C; relative humidity >80%), animal body

temperature, a surrogate for alveolar temperature, was estimated (37.5°C) for both groups in our study for the purpose of the calculation of tidal volume. This additional limitation raises concern over the accuracy of our estimation of tidal volume, important to address since we report that tidal volume was significantly different between wild-type and *mdx* mice. Direct airflow measurement with a pneumotachometer or assessment of breathing using head-out plethysmography would provide accurate measures of tidal volumes, worthy of pursuit into the future, although it is recognized that these techniques are not without limitations associated with anaesthesia and restraint, respectively. Of note for the present study, errors in body temperature could conceivably have accounted for a substantive proportion of the difference reported between wild-type and *mdx* mice (Mortola & Frappell, 1998). We determined that basal CO_2 production was equivalent in both groups, but we assumed for the purpose of tidal volume calculation that body temperature was also equivalent, which we acknowledge is an assumption of major significance in the calculation of tidal volume. We report a significant decrease in CO_2 production during both sustained and graded hypoxia. Body temperature also likely decreased during the hypoxic challenges. Whereas, the hypometabolic response (decreased CO_2 production) was equivalent in wild-type and *mdx* mice, we assumed (because we did not measure) that the likely hypothermic response was also equivalent between wild-type and *mdx* mice. Our assumption does not account for potential differences in body temperature between wild-type and *mdx* mice at rest and/or in response to gas challenge. Of interest, a significant difference in resting body temperature between wild-type and *mdx* mice was reported in a previous study (Helliwell *et al*., 1996). However, such a difference if it existed in our study would on average have resulted in an under-estimation of the magnitude of the reduction in tidal volume in *mdx* mice compared with wild-type during normoxia. It is also probable that our use of a single estimated body temperature for all animals in the study introduced errors and thus variability within and not just between groups, with potential consequences for comparisons between groups. It remains possible that a component ---perhaps substantial --- of the difference in tidal volume reported in the present study relates to differences in body temperature between wild-type and *mdx* mice and hence errors related to the assumptions made herein. This issue should be addressed in future studies, notwithstanding the inherent limitations of the technique of whole-body plethysmography for the estimation of tidal volume even with incorporation of body temperature. If differences exist in body temperature between wild-type and mdx mice, and their respective hypothermic response to hypoxia, this would be a fruitful area worthy of investigation.

We acknowledge the apparent discrepancy in the strength of the conclusions drawn from plethysmography and intra-cardiac blood gas analysis, particularly in the light of the limitations described above. We have favoured the conclusion that *mdx* animals hypoventilate based on the

significant decrease in V_E/VCO_2 measurements derived by plethysmography. Yet, the blood gas data, which are ordinarily taken as the gold standard, suggest modest differences in PO_2 and PCO_2 but with additional supporting evidence suggesting a compensated respiratory acidosis. We suggest that blood gas data should be viewed cautiously in our study, acknowledging that sample size was a limiting factor, but again we emphasize that the magnitude of the hypoventilation reported in our study by use of whole-body plethysmography may have been over-estimated. If ventilatory capacity is preserved in *mdx*, it is an impressive feat considering the profound diaphragm weakness that is evident in the model at an early age. Arterial blood gas sampling in conscious mice during ventilatory and metabolic assessment by plethysmography represents the gold standard for comparisons and would be required to convincingly demonstrate hypoventilation in young *mdx* mice.

Our EMG study suggests compensatory neuroplasticity in respiratory motor output in *mdx* mice in response to chemostimulation. We acknowledge that recordings of respiratory motor nerves in reduced preparations, complemented by respiratory EMGs in intact spontaneously breathing preparations, extending to contemporaneous recordings of respiratory EMGs and breathing across the sleep-wake cycle would lend further credence to this novel observation.

Relevance to DMD

Our study in the *mdx* mouse raises interesting issues of potential relevance to human DMD. Dystrophin deficiency results in respiratory insufficiency early in life, which could establish blood gas disturbances with relevance to neuromuscular performance. Hypoxia-induced respiratory muscle dysfunction may be an important and under-recognised feature of DMD. Dystrophin deficiency may adversely affect basal sensory control of breathing, but the preserved capacity for carotid body chemoafferents to respond to hypoxia and therefore presumably other stimulants, suggests that pharmacotherapies that enhance carotid body activity may have some application in the treatment of DMD. It is apparent that dystrophin deficiency results in profound diaphragm dysfunction, which appears early in the mouse model. The severe mechanical disadvantage presents across a range of stimulations, but a preserved capacity to raise ventilation suggests support from accessory muscles of breathing, which may have relevance to DMD. Our study revealed a potentiated neural drive to breathe in *mdx* during maximal chemoactivation, suggesting compensatory neuroplasticity enhancing respiratory motor output to the diaphragm and perhaps other respiratory muscles, which should serve to facilitate ventilation in response to challenge. If neuroplasticity is a feature of DMD, it may be possible to boost motor facilitation of breathing through safe interventions, and in this way preserve or limit deficiencies in respiratory capacity.

5. References

Bavis RW, van Heerden ES, Brackett DG, Harmeling LH, Johnson SM, Blegen HJ, Logan S, Nguyen GN & Fallon SC. (2014). Postnatal development of eupneic ventilation and metabolism in rats chronically exposed to moderate hyperoxia. *Respir Physiol Neurobiol* **198,** 1-12.

Bavis RW, Young KM, Barry KJ, Boller MR, Kim E, Klein PM, Ovrutsky AR & Rampersad DA. (2010). Chronic hyperoxia alters the early and late phases of the hypoxic ventilatory response in neonatal rats. *J Appl Physiol (1985)* **109,** 796-803.

Baydur A, Gilgoff I, Prentice W, Carlson M & Fischer DA. (1990). Decline in respiratory function and experience with long-term assisted ventilation in advanced Duchenne's muscular dystrophy. *Chest* **97,** 884-889.

Beck J, Weinberg J, Hamnegård CH, Spahija J, Olofson J, Grimby G & Sinderby C. (2006). Diaphragmatic function in advanced Duchenne muscular dystrophy. *Neuromuscul Disord* **16,** 161-167.

Bersanini C, Khirani S, Ramirez A, Lofaso F, Aubertin G, Beydon N, Mayer M, Maincent K, Boulé M & Fauroux B. (2012). Nocturnal hypoxaemia and hypercapnia in children with neuromuscular disorders. *Eur Respir J* **39,** 1206-1212.

Burns DP, Edge D, O'Malley D & O'Halloran KD. (2015). Respiratory control in the mdx mouse model of Duchenne muscular dystrophy. *Adv Exp Med Biol* **860,** 239-244.

Burns DP & O'Halloran KD. (2016). Evidence of hypoxic tolerance in weak upper airway muscle from young mdx mice. *Respir Physiol Neurobiol* **226,** 68-75.

Burns DP, Rowland J, Canavan L, Murphy KH, Brannock M, O'Malley D, O'Halloran KD & Edge D. (2017). Restoration of pharyngeal dilator muscle force in dystrophin deficient (mdx) mice following co-treatment with neutralizing IL-6 receptor antibodies and Urocortin-2. *Exp Physiol*, doi: 10.1113/EP086232.

Christakos CN, Cohen MI, Barnhardt R & Shaw CF. (1991). Fast rhythms in phrenic motoneuron and nerve discharges. *J Neurophysiol* **66,** 674-687.

Coirault C, Pignol B, Cooper RN, Butler-Browne G, Chabrier PE & Lecarpentier Y. (2003). Severe muscle dysfunction precedes collagen tissue proliferation in mdx mouse diaphragm. *J Appl Physiol (1985)* **94,** 1744-1750.

De Bruin PF, Ueki J, Bush A, Khan Y, Watson A & Pride NB. (1997). Diaphragm thickness and inspiratory strength in patients with Duchenne muscular dystrophy. *Thorax* **52,** 472-475.

Deconinck N & Dan B. (2007). Pathophysiology of duchenne muscular dystrophy: current hypotheses. *Pediatr Neurol* **36,** 1-7.

Dubach-Powell J. (2008). Quantitative determination of muscle fibre diameter (minimal Feret's diameter) and percentage of centralised nuclei, pp. 14. TREAT-NMD Neuromuscular Network.

ElMallah MK, Stanley DA, Lee KZ, Turner SM, Streeter KA, Baekey DM & Fuller DD. (2016). Power spectral analysis of hypoglossal nerve activity during intermittent hypoxia-induced long-term facilitation in mice. *J Neurophysiol* **115,** 1372-1380.

Ervasti JM. (2007). Dystrophin, its interactions with other proteins, and implications for muscular dystrophy. *Biochim Biophys Acta* **1772,** 108-117.

Fuller DD & Mitchell GS. (2017). Respiratory neuroplasticity - Overview, significance and future directions. *Exp Neurol* **287,** 144-152.

Gayraud J, Matecki S, Hnia K, Mornet D, Prefaut C, Mercier J, Michel A & Ramonatxo M. (2007). Ventilation during air breathing and in response to hypercapnia in 5 and 16 month-old mdx and C57 mice. *J Muscle Res Cell Motil* **28,** 29-37.

Han JJ, Carter GT, Ra JJ, Abresch RT, Chamberlain JS & Robinson LR. (2006). Electromyographic studies in mdx and wild-type C57 mice. *Muscle Nerve* **33,** 208-214.

Haouzi P, Bell HJ, Notet V & Bihain B. (2009). Comparison of the metabolic and ventilatory response to hypoxia and H2S in unsedated mice and rats. *Respir Physiol Neurobiol* **167,** 316-322.

Helliwell TR, MacLennan PA, McArdle A, Edwards RH & Jackson MJ. (2006). Fasting increases the extent of muscle necrosis in the mdx mouse. CLin Sci 90, 467-472.

Huang P, Cheng G, Lu H, Aronica M, Ransohoff RM & Zhou L. (2011). Impaired respiratory function in mdx and mdx/utrn(+/-) mice. *Muscle Nerve* **43,** 263-267.

Ishizaki M, Suga T, Kimura E, Shiota T, Kawano R, Uchida Y, Uchino K, Yamashita S, Maeda Y & Uchino M. (2008). Mdx respiratory impairment following fibrosis of the diaphragm. *Neuromuscul Disord* **18,** 342-348.

Khirani S, Ramirez A, Aubertin G, Boulé M, Chemouny C, Forin V & Fauroux B. (2014). Respiratory muscle decline in Duchenne muscular dystrophy. *Pediatr Pulmonol* **49,** 473-481.

Kim JH, Kwak HB, Thompson LV & Lawler JM. (2013). Contribution of oxidative stress to pathology in diaphragm and limb muscles with Duchenne muscular dystrophy. *J Muscle Res Cell Motil* **34,** 1-13.

Kim JH & Lawler JM. (2012). Amplification of proinflammatory phenotype, damage, and weakness by oxidative stress in the diaphragm muscle of mdx mice. *Free Radic Biol Med* **52,** 1597-1606.

Kline DD, Peng YJ, Manalo DJ, Semenza GL & Prabhakar NR. (2002). Defective carotid body function and impaired ventilatory responses to chronic hypoxia in mice partially deficient for hypoxia-inducible factor 1 alpha. *Proc Natl Acad Sci U S A* **99,** 821-826.

Kumar P & Prabhakar NR. (2012). Peripheral chemoreceptors: function and plasticity of the carotid body. *Compr Physiol* **2,** 141-219.

Lewis P, Sheehan D, Soares R, Coelho AV & O'Halloran KD. (2016). Redox remodeling is pivotal in murine diaphragm muscle adaptation to chronic sustained hypoxia. *Am J Respir Cell Mol Biol* **55,** 12-23.

Lewis P, Sheehan D, Soares R, Varela Coelho A & O'Halloran KD. (2015). Chronic sustained hypoxia-induced redox remodeling causes contractile dysfunction in mouse sternohyoid muscle. *Front Physiol* **6,** 122.

Lidov HG. (1996). Dystrophin in the nervous system. *Brain Pathol* **6,** 63-77.

McMorrow C, Fredsted A, Carberry J, O'Connell RA, Bradford A, Jones JF & O'Halloran KD. (2011). Chronic hypoxia increases rat diaphragm muscle endurance and sodium-potassium ATPase pump content. *Eur Respir J* **37,** 1474-1481.

Melacini P, Vianello A, Villanova C, Fanin M, Miorin M, Angelini C & Dalla Volta S. (1996). Cardiac and respiratory involvement in advanced stage Duchenne muscular dystrophy. *Neuromuscul Disord* **6,** 367-376.

Mitchell GS & Johnson SM. (2003). Neuroplasticity in respiratory motor control. *J Appl Physiol (1985)* **94,** 358-374.

Mortola JP & Frappell PB. (1998). On the barometric method for measurements of ventilation, and its use in small animals. *Can J Physiol Pharmacol* **76,** 937-944.

Mosqueira M, Baby SM, Lahiri S & Khurana TS. (2013a). Ventilatory chemosensory drive is blunted in the mdx mouse model of Duchenne Muscular Dystrophy (DMD). *PLoS One* **8,** e69567.

Mosqueira M, Zeiger U, Förderer M, Brinkmeier H & Fink RH. (2013b). Cardiac and respiratory dysfunction in Duchenne muscular dystrophy and the role of second messengers. *Med Res Rev* **33,** 1174-1213.

Muntoni F, Torelli S & Ferlini A. (2003). Dystrophin and mutations: one gene, several proteins, multiple phenotypes. *Lancet Neurol* **2,** 731-740.

O'Neal MH, Spiegel ET, Chon KH & Solomon IC. (2005). Time-frequency representation of inspiratory motor output in anesthetized C57BL/6 mice in vivo. *J Neurophysiol* **93,** 1762-1775.

Pratt SJ, Valencia AP, Le GK, Shah SB & Lovering RM. (2015). Pre- and postsynaptic changes in the neuromuscular junction in dystrophic mice. *Front Physiol* **6,** 252.

Roy A, Mandadi S, Fiamma MN, Rodikova E, Ferguson EV, Whelan PJ & Wilson RJ. (2012). Anandamide modulates carotid sinus nerve afferent activity via TRPV1 receptors increasing responses to heat. *J Appl Physiol (1985)* **112,** 212-224.

Shortt CM, Fredsted A, Chow HB, Williams R, Skelly JR, Edge D, Bradford A & O'Halloran KD. (2014). Reactive oxygen species mediated diaphragm fatigue in a rat model of chronic intermittent hypoxia. *Exp Physiol* **99,** 688-700.

Skelly JR, Edge D, Shortt CM, Jones JF, Bradford A & O'Halloran KD. (2012). Tempol ameliorates pharyngeal dilator muscle dysfunction in a rodent model of chronic intermittent hypoxia. *Am J Respir Cell Mol Biol* **46,** 139-148.

Smith PE, Edwards RH & Calverley PM. (1989a). Oxygen treatment of sleep hypoxaemia in Duchenne muscular dystrophy. *Thorax* **44,** 997-1001.

Smith PE, Edwards RH & Calverley PM. (1989b). Ventilation and breathing pattern during sleep in Duchenne muscular dystrophy. *Chest* **96,** 1346-1351.

Stephenson R & Gucciardi EJ. (2002). Theoretical and practical considerations in the application of whole body plethysmography to sleep research. *Eur J Appl Physiol* **87,** 207-219.

Wilson RJ & Teppema LJ. (2016). Integration of central and peripheral respiratory chemoreflexes. *Compr Physiol* **6,** 1005-1041.

6. Additional information

Competing Interests

The authors have no financial, professional or personal conflicts relating to this publication.

Author Contributions

DPB: experimental design; acquisition of data; data and statistical analysis and interpretation of data; drafting of the original manuscript; AR: carotid body studies: experimental design; acquisition

of data; analysis; drafting of the original manuscript; DE: muscle histology: experimental design; data acquisition; interpretation of data; SG: muscle histology: data acquisition; data analysis; EFL: experimental design; acquisition of data; FBMcD: carotid body studies: experimental design; analysis; RJW: carotid body studies: experimental design; critical revision of the manuscript for important intellectual content; KDOH: experimental design; statistical analysis and interpretation of data; drafting and critical revision of the manuscript for important intellectual content.

Funding

DPB was supported by funding from the Department of Physiology, UCC. Salary support for RJW provided by Alberta Innovates Health Solutions and work in Calgary was funded by the Canadian Institutes for Health Research.

Acknowledgements

We are grateful to staff of the Biological Services Unit, University College Cork for their support in the breeding and maintenance of the murine colonies.

Translational Perspective

Duchenne muscular dystrophy (DMD) is an X-linked fatal neuromuscular disease, which commonly culminates in respiratory failure. Whereas respiratory muscle dysfunction is recognized in DMD, a comprehensive assessment of respiratory control is lacking. The dystrophin-deficient *mdx* mouse has proved to be a useful pre-clinical model of DMD, principally because diaphragm muscle dysfunction recapitulates features of the human disease. We set out to interrogate sensory and motor control of breathing in young *mdx* mice. We hypothesized that there would be evidence of plasticity in the neural control of breathing. Our study reveals that *mdx* mice hypoventilate as early as 8 weeks of age (equivalent to young adult). We revealed evidence of sensory deficit in *mdx* mice which may partly contribute to resting hypoventilation, but sensory responses to oxygen deprivation (hypoxia) are normal. Ventilatory responses to respiratory-relevant chemical activation of breathing are normal in *mdx* mice, revealing ventilatory reserve, although ventilation is lower in *mdx* mice compared with wild-type mice at all levels of ventilation. Assessment of diaphragm electromyogram activity revealed enhanced motor drive to the respiratory pump muscle during maximum chemoactivation, revealing a compensatory phenomenon in neuromechanical control of ventilation in *mdx* mice. Profound diaphragm weakness in young *mdx* mice suggests that enhanced recruitment of accessory muscles of breathing may be especially important in facilitating enhanced lung ventilation during chemoactivation. Our novel findings have implications for human DMD. Safe interventional therapies that serve to boost breathing may preserve or limit deficiencies in respiratory capacity in DMD patients reducing morbidity and mortality.

Translational Perspective Word Count = 249

Table legends

Table 1. Baseline ventilation and metabolic measurements

	WT (n=13)	***mdx* (n=12)**	**Student *t* tests**
VO_2 (ml/min)	1.6 ± 0.2	1.5 ± 0.3	*P* = 0.6985
VO_2 (ml/g/min)	0.072 ± 0.01	0.058 ± 0.01	*P* = 0.0043
VCO_2 (ml/min)	0.86 ± 0.18	0.94 ± 0.25	*P* = 0.3570
VCO_2 (ml/g/min)	0.040 ± 0.009	0.036 ± 0.009	*P* = 0.2404
VCO_2/VO_2	0.6 ± 0.1	0.6 ± 0.1	*P* = 0.2228
V_E/VO_2	17.5 ± 5.4	13.6 ± 5.5	*P* = 0.0819
V_E/VCO_2	32.4 ± 11.5	22.4 ± 8.8	*P* = 0.0243
Body mass (g)	22.0 ± 1.7	26.3 ± 1.4	*P* < 0.0001

Definition of abbreviations: VO_2, oxygen consumption; VCO_2, carbon dioxide production; VCO_2/VO_2, respiratory exchange ratio (RER); V_E/VO_2, ventilatory equivalent for O_2; V_E/VCO_2, ventilatory equivalent for CO_2; WT, wild-type. Data are shown as mean±SD and were statistically compared using unpaired Student *t* tests.

Table 2. Intra-cardiac blood gas analysis

	WT (n=7)	*mdx* (n=7)	Student *t* tests
pH	7.37 ± 0.03	7.37 ± 0.01	*P* = 0.5815
PCO_2 (mmHg)	35.2 ± 4.7	38.3 ± 2.0	*P* = 0.1248
PO_2 (mmHg)	107.1 ± 13.7	96.7 ± 6.2	*P* = 0.0920
HCO_3^- (mmol/L)	20.0 ± 2.4	22.3 ± 1.4	*P* = 0.0496
TCO_2 (mmol/L)	21.0 ± 2.4	23.4 ± 1.4	*P* = 0.0382
SaO_2 (%)	97.9 ± 0.9	97.3 ± 0.8	*P* = 0.2225
Na^+ (mmol/L)	143.0 ± 1.2	144.1 ± 0.7	*P* = 0.0442
K^+ (mmol/L)	4.4 ± 0.2	5.0 ± 0.4	*P* = 0.0078
Haematocrit (%)	39.7 ± 1.4	36.0 ± 1.5	*P* = 0.0005
Hb (g/dl)	13.5 ± 0.5	13.0 ± 2.1	*P* = 0.5080

Definition of abbreviations: PCO_2, partial pressure of CO_2; PO_2, partial pressure of O_2; HCO_3^-, bicarbonate; TCO_2, total CO_2; SaO_2, arterial oxygen saturation; Na^+, sodium; K^+, potassium; Hb, haemoglobin; WT, wild-type. Data are shown as mean±SD and were statistically compared using unpaired Student *t* tests.

Table 3. Carotid sinus nerve afferent discharge in normoxia and hypoxia

		100 mmHg	80 mmHg	60 mmHg	40 mmHg	Two-way RMANOVA
Discharge frequency (impulses/min)	WT	37.4 ± 20.7	53.2 ± 23.9	82.3 ± 39.9	122.2 ± 73.1	Gas $P < 0.001$ Gene $P = 0.327$ Gas x gene $P = 0.953$
	mdx	23.8 ± 11.5	36.2 ± 14.5	54.9 ± 22.4	80.0 ± 39.6	
Δ discharge frequency (impulses/min)	WT	-	15.8 ± 7.8	44.9 ± 26.2	84.8 ± 59.6	Gas $P < 0.001$ Gene $P = 0.357$ Gas x gene $P = 0.228$
	mdx	-	12.5 ± 8.1	31.3 ± 16.2	56.3 ± 36.2	

Definition of abbreviations: WT, wild-type. Data are shown as mean±SD and were statistically compared by repeated measures two-way ANOVA (gas x gene). Responses to hypoxia are expressed as Δ impulses per min from baseline (normoxia) values.

Table 4. Diaphragm muscle twitch force and contractile kinetics

	WT (n=7)	*mdx* (n=7)	Student *t* tests
CT (ms)	15.4 ± 1.3	18.9 ± 3.0	$P = 0.0155$
½ RT (ms)	19.9 ± 3.0	19.1 ± 2.9	$P = 0.5975$
P_t (N/cm^2)	2.7 ± 0.7	1.8 ± 0.8	$P = 0.0292$

Definition of abbreviations: CT, contraction time; ½ RT, half-relaxation time; P_t, twitch force; WT, wild-type. Data are shown as mean±SD and were statistically compared using unpaired Student *t* tests.

Figure legends

Figure 1. Baseline ventilation in conscious mice

A: representative respiratory flow traces during normoxic ventilation in a wild-type mouse (black) and *mdx* mouse (grey); inspiration downwards. B, C and D: breathing frequency (B), tidal volume (C) and minute ventilation (D) for wild-type (WT) (n=13) and *mdx* (n=12) mice during normoxic ventilation. Values (B-D) are expressed as box and whisker plots (median, 25-75% centiles and minimum and maximum values) and data were statistically compared by unpaired Student *t* tests with Welch's correction used where appropriate. ***P<0.001 compared with WT.

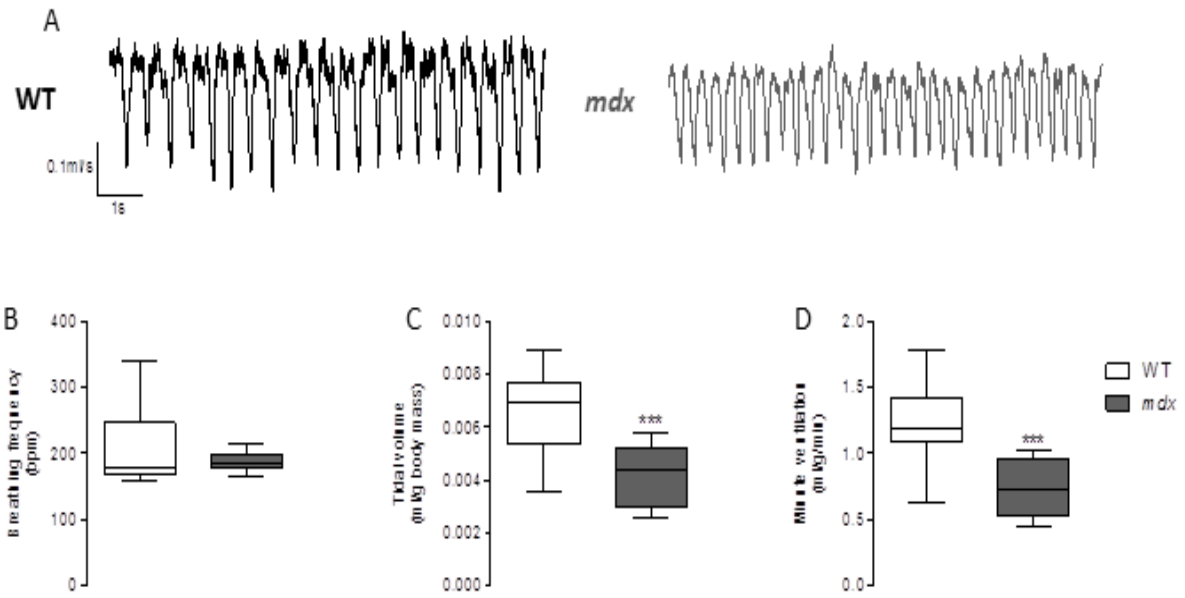

Figure 2. *Ex vivo* carotid sinus nerve discharge

A and B: representative recordings of integrated carotid sinus nerve (CSN) activity *ex vivo* in a wild-type mouse (A) and *mdx* mouse (B) during normoxia (100 mmHg) and mild (80 mmHg), moderate (60 mmHg) and severe (40 mmHg) hypoxia. CSN activity was normalized to activity in hyperoxia (500 mmHg), illustrated by the horizontal dashed line. C: group data of CSN activity for wild-type (WT, n=6) and *mdx* (n=6) during normoxia (100 mmHg) and graded hypoxia (80, 60, 40 mmHg). Values are expressed as box and whisker plots (median, 25-75% centiles and minimum and maximum values). Data were statistically compared by repeated measures two-way ANOVA (gas x gene).

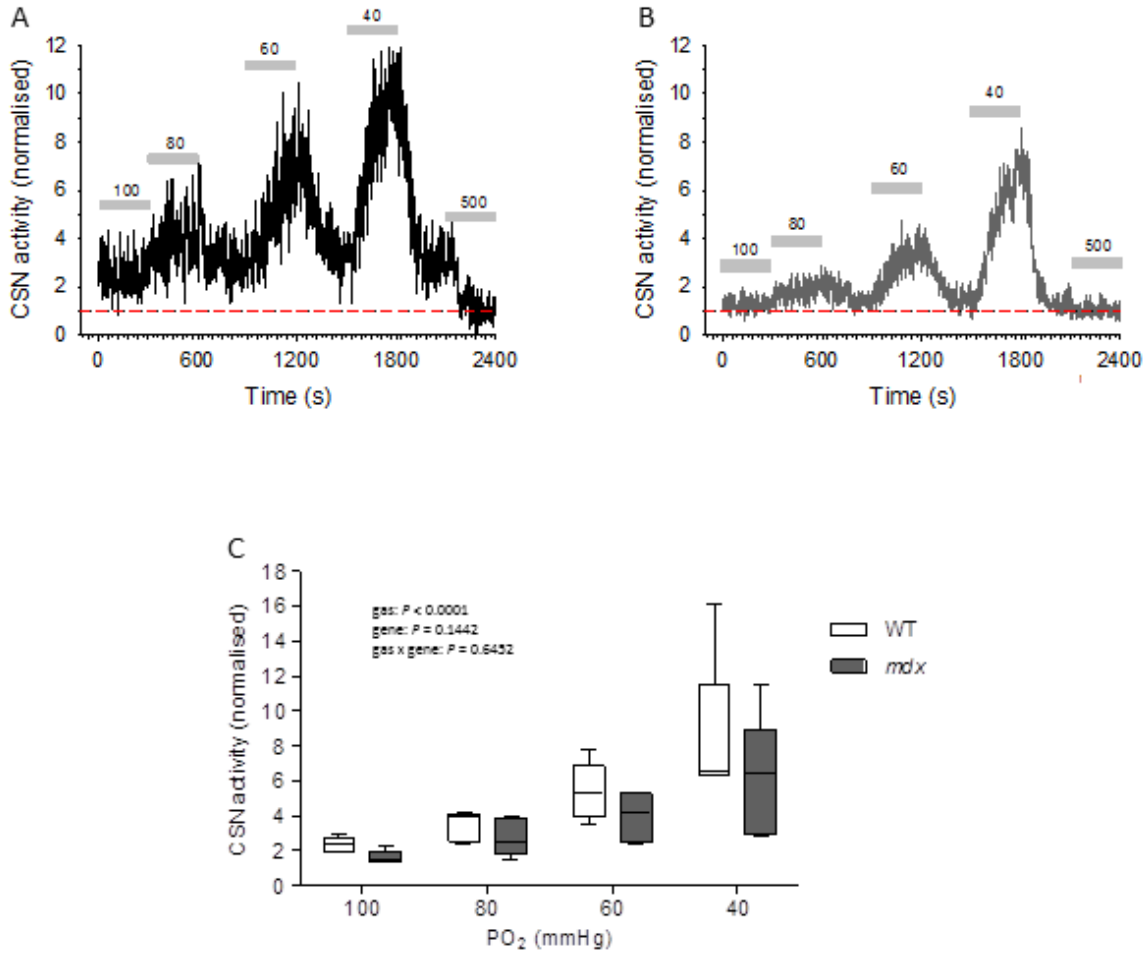

Figure 3. Ventilatory and metabolic responsiveness to graded hypoxia

A-H: group data for breathing frequency (A), tidal volume (B), minute ventilation (C), oxygen consumption (D; VO_2), carbon dioxide production (E; VCO_2), respiratory exchange ratio (F; VCO_2/VO_2), ventilatory equivalent for oxygen (G; V_E/VO_2) and ventilatory equivalent for carbon dioxide (H; V_E/VCO_2) for wild-type (WT, n=13) and *mdx* (n=12) mice during normoxia (21% inspired O_2; balance N_2) and graded hypoxia (15, 12, 10 and 8% inspired O_2; balance N_2). Values expressed as box and whisker plots (median, 25-75% centiles and minimum and maximum values). Data were

statistically compared by repeated measures two-way ANOVA (gas x gene) with Bonferroni post hoc test. *P<0.05, **P<0.01 compared with corresponding WT value.

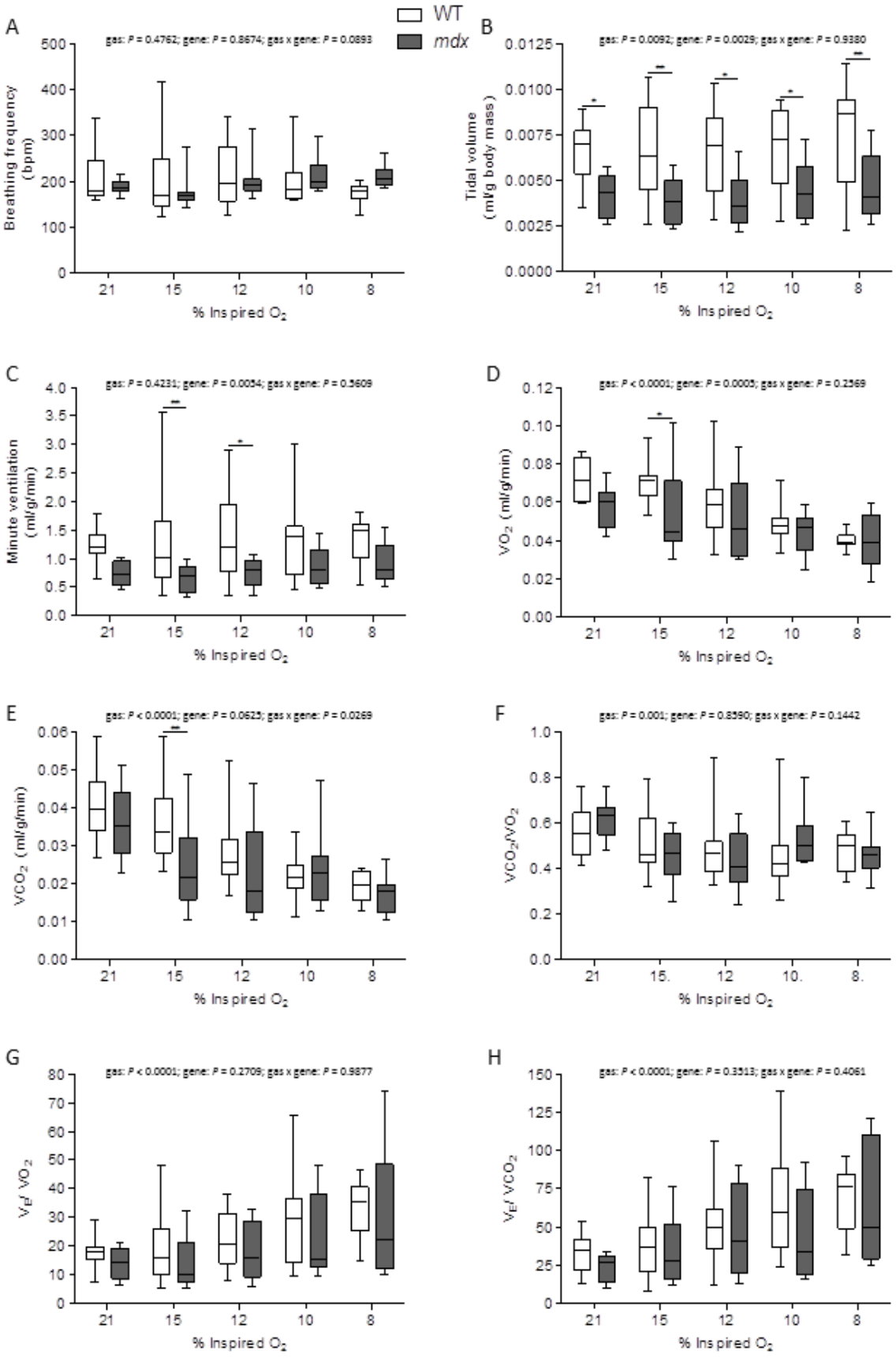

Figure 4. Ventilatory and metabolic responsiveness to sustained hypoxia

A-H: group data (mean±SD) for breathing frequency (A), tidal volume (B), minute ventilation (C), oxygen consumption (D; VO_2), carbon dioxide production (E; VCO_2), respiratory exchange ratio (F; VCO_2/VO_2), ventilatory equivalent for oxygen (G; V_E/VO_2) and ventilatory equivalent for carbon dioxide (H; V_E/VCO_2) for wild-type (WT, n=13) and *mdx* (n=12) mice during baseline and after 5-20 minutes of exposure to hypoxia (10% O_2 inspired oxygen; balance N_2). Data were statistically compared by repeated measures two-way ANOVA (gas x gene) with Bonferroni post-hoc test. **P*<0.05, ***P*<0.01 compared with corresponding WT value.

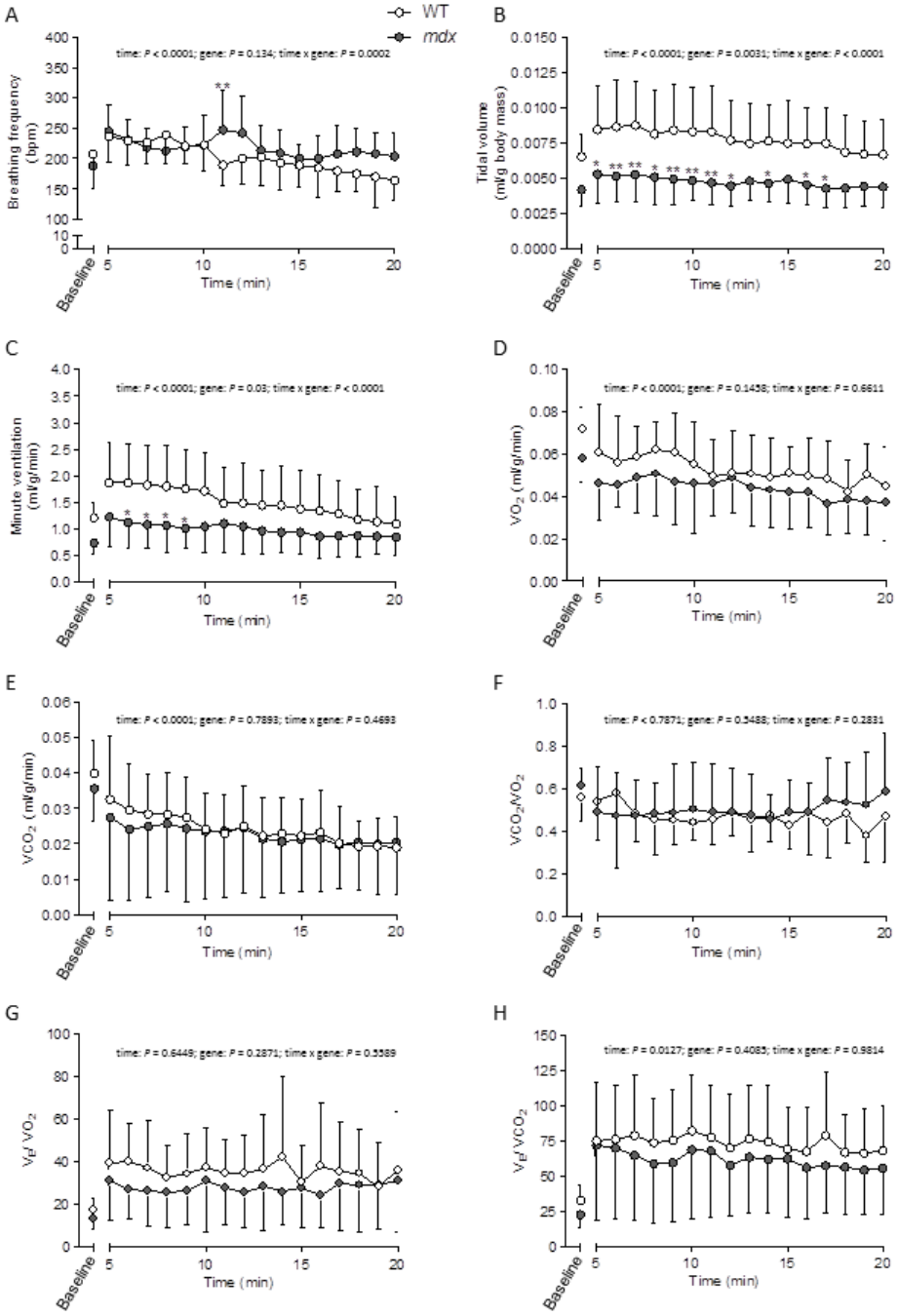

Figure 5. Ventilatory responsiveness to hypercapnia

A: group data (mean±SD) for minute ventilation in wild-type (WT, n=10) and *mdx* (n=11) mice during baseline (air) and hypercapnia (5% CO_2, balance N_2). Data were statistically compared using repeated measures two-way ANOVA. B: group data (mean±SD) for ventilatory responsiveness to hypercapnia (ΔV_E) in WT (n=10) and *mdx* (n=11) mice. Values are expressed as box and whisker plots (median, 25-75% centiles and minimum and maximum values). Data were statistically compared by unpaired Student *t* tests.

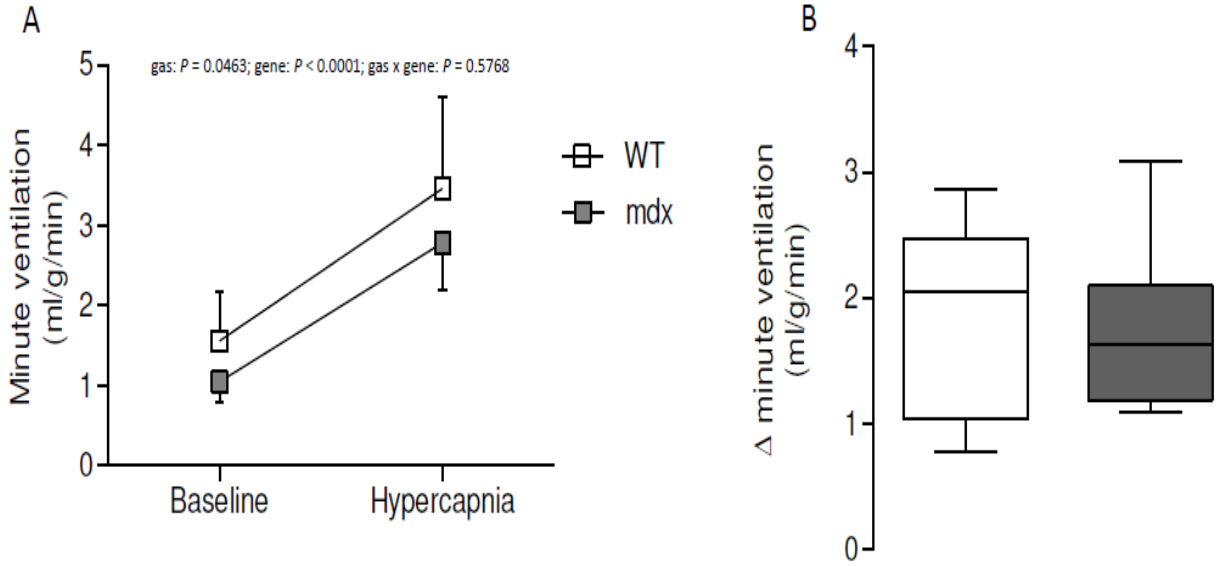

Figure 6. *Ex vivo* diaphragm muscle contractile function

A and B: original traces of *ex vivo* diaphragm muscle twitch contraction (A) and force-frequency relationship (B) for wild-type (WT) (black) and *mdx* (grey) preparations. C, group data (mean ± SD; n=7 for both groups) for diaphragm muscle force-frequency relationship *ex vivo* in WT (open) and *mdx* (grey) muscle preparations. Data were statistically compared by repeated measures two-way ANOVA (frequency x gene) followed by Bonferroni post-hoc test. ***P* < 0.01, ****P* < 0.001 compared with corresponding WT value.

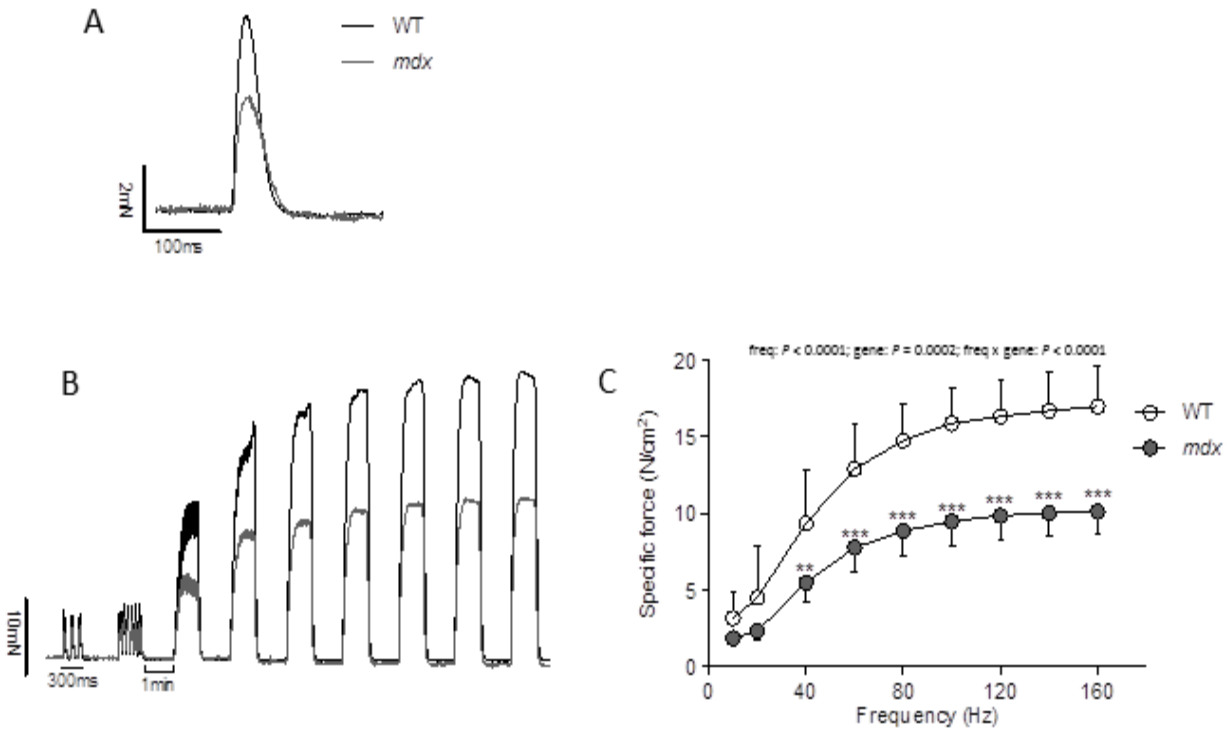

Figure 7. Diaphragm muscle structure

A: representative images of diaphragm muscle immunofluorescently labelled for laminin from wild-type (WT) (top left) and *mdx* (top right) mice. B: representative images of diaphragm muscle immunofluorescently labelled for laminin (green) and myonuclei (blue) from WT (bottom left) and *mdx* (bottom right) mice. C: group data for coefficient of variation of diaphragm muscle fibre size as measured by minimal Feret's diameter for WT (n=8) and *mdx* (n=8) mice. D: group data for percentage of fibres with centralized myonuclei in diaphragm muscle of WT (n=6) and *mdx* (n=5) mice. Values are expressed as box and whisker plots (median, 25-75% centiles and minimum and maximum values). Data were statistically compared by unpaired Student *t* tests. E and F: frequency distribution of WT and *mdx* diaphragm muscle fibre size as measured by minimal Feret's diameter

(E) and cross-sectional area (F). ***P = 0.0005, ****P < 0.0001 compared with corresponding WT value.

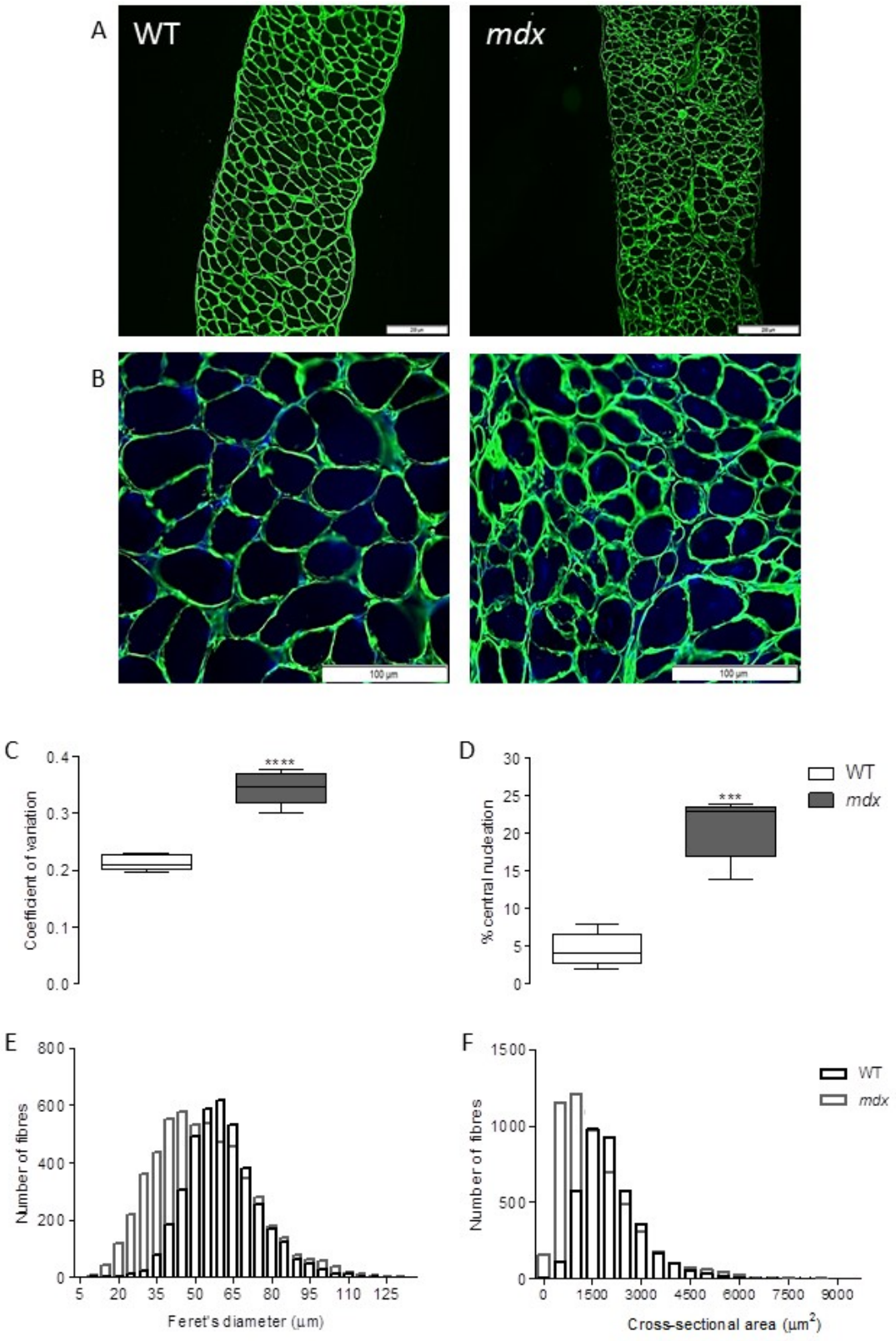

Figure 8. Diaphragm EMG

A: representative traces of diaphragm (Dia) muscle raw and integrated (Int.) EMG activity for a wild-type (WT) mouse (black) and *mdx* mouse (grey) during baseline (60% inspired O_2), hypercapnia (5% and 10% CO_2), hypoxia (15% O_2) and asphyxia (15% O_2/5% CO_2). B and C: diaphragm muscle integrated EMG activity expressed as amplitude (B) and area under the curve (C) for WT (n=8) and *mdx* (n=7) mice during baseline (inset), hypercapnia (5% CO_2 and 10% CO_2), hypoxia (15% O_2) and asphyxia (15% O_2/5% CO_2). Baseline data are reported as absolute units. Note that there was no significant difference in baseline data comparing WT and *mdx* mice. Gas challenges are expressed as % change from baseline. All values are presented as box and whisker plots (median, 25-75% centiles and minimum and maximum values). Baseline data were statistically compared by unpaired Student *t* tests. Gas challenges were statistically compared by repeated measures two-way ANOVA with Bonferroni post-hoc test. **P* < 0.05 compared with WT.